Int. J. Electrochem. Sci., 15 **(2020)** 7423 – 7433, doi: 10.20964/2020.08.52

International Journal of
ELECTROCHEMICAL
SCIENCE
www.electrochemsci.org

In situ fabrication of Cu-bipy-BTC Metal-organic Framework Electrode for Catechol Detection

Zhipeng LI[1], *Liwei Ren*[2,*] *and Diannan Lu*[1,*]

[1] Key Lab of Industrial Biocatalysis, Ministry of Education, China, Department of Chemical Engineering, Tsinghua University, Beijing, China
[2] College of Biological and Pharmaceutical Sciences, Three Gorges University, Yichang, Hubei Province, China
[*]E-mail: ludiannan@tsinghua.edu.cn.com (D.L.); renliwei@ctgu.edu.cn (L.R.)

Received: 13 May 2020 / *Accepted:* 27 May 2020 / *Published:* 10 July 2020

In this work, the metal organic frameworks (MOFs) Cu-bipy-BTC ($[Cu_2(OH)(2,2'\text{-bipy})_2(BTC)_3 2H_2O]_n$) were *in situ* synthesized on the surface of a gold electrode directly to form a hybrid material of a $Cu(OH)_2$ nanosheet and Cu-bipy-BTC nanoparticle. The structure of this hybrid material on the electrode surface was characterized using Fourier-transform infrared spectroscopy, X-ray diffraction, scanning electron microscopy, and energy-dispersive spectrocopy. It is shown that the newly *in situ* synthesized Cu-bipy-BTC MOF can serve as active metal centers, and is embedded in different hydrophobic environments formed by $Cu(OH)_2$ nanosheets. This unique structure is very similar to that of an active site of laccase, giving better catalytic activity. This MOF-based electrode enables the catalytic oxidation of catechol at +0.4 V (versus Ag/AgCl). The amperometric responses are linear with concentrations of catechol ranging from 10 to 250 μM and 250 to 1000 μM with sensitivities of 1.6224 and 0.2591 $\mu A \cdot cm^{-2} \cdot \mu M^{-1}$, respectively. Compared with other catechol electrochemical sensors, this MOF-based electrode has advantages of higher sensitivity and easy manufacturability, facilitating its potential application in the detection of catechol.

Keywords: hybrid structure, asymmetry Cu-bipy-BTC MOF, $Cu(OH)_2$ nanosheet, *in situ* fabrication, electro-catalysis, catechol detection

1. INTRODUCTION

Laccases are a kind of multi-copper oxidase enzyme that catalyzes the oxidation of various inorganics and aromatic substances (especially phenols) while reducing oxygen to water concomitantly [1]. In general, there are four copper atoms per active protein unit, which can be classified into three types [2]. Oxidation of the substrate takes place at the T1 copper site with a high redox potential of +790 mV. The trinuclear cluster formed by T2 and T3 coppers is the site that reduces oxygen to water [3]. The

T1 copper site has a higher redox potential because of the asymmetric coordinate structure of copper ions, including longer Cu-N bond length and a planar triangular coordinate lacking a fourth coordinated residue and hydrophobic residues around it [4, 5].

Phenolic compounds are widely used worldwide, but are frequently leaked, which can cause environmental pollution. Among these compounds, pyrocatechols or catechols deserve special attention because they can cause damage to a variety of biomolecules such as DNA, proteins, and membranes, by ultimately reacting with them [6]. The common methods of detecting such compounds, such as spectrophotometry and gas chromatography, which need derivatization and pre-concentration steps, are often complicated and expensive [7]. Owing to the aforementioned structural characteristics, laccase biosensors have unique merits, e.g., ease of use, speed, accuracy, high sensitivity, a broad substrate spectrum, and high turnover number [8,9]. However, several disadvantages, including temperature influence, stability at different conditions, and the high cost of laccase, limit their use.

Metal-organic frameworks (MOFs), a kind of emerging new porous material, were first introduced by Yaghi *et al*. in 1995 [10]. MOFs are compounds composed of metal centers or clusters coordinated to organic ligands. MOFs have been widely used in several different fields, such as sensors, storage and separation of gas or liquid, catalysts, and drug delivery [11]. Considering the unique properties and functions of MOFs, they have also been studied to imitate the functionalities of natural biological systems [12]. Cu-bipy-BTC ($[Cu_2(OH)(2,2'\text{-bipy})_2(BTC)_3\ 2H_2O]_n$), first reported by Song *et al*., was synthesized to sense the leakage of methanol [13]; its structure is shown in Figure 1(b). Since then, such MOFs have been used in the oxygen reduction reaction (ORR) [14–17], electrocatalytic oxidative carbonylation of methane to dimethyl carbonate [15,18], and in electrochemical storage devices [19]. In these works, Cu-bipy-BTC is synthesized via a hydrothermal method and dip-coated onto the electrode surface.

In the present study, Cu-bipy-BTC was directly prepared on the surface of Au electrode *in situ*. The synthesized Cu-bipy-BTC has a structure similar to that of the T1 copper site of laccase, as shown in Figure 1. Finally, this electrode was used to mimic the function of laccase, achieving the biomimetic catalysis and detection of phenols quantitatively.

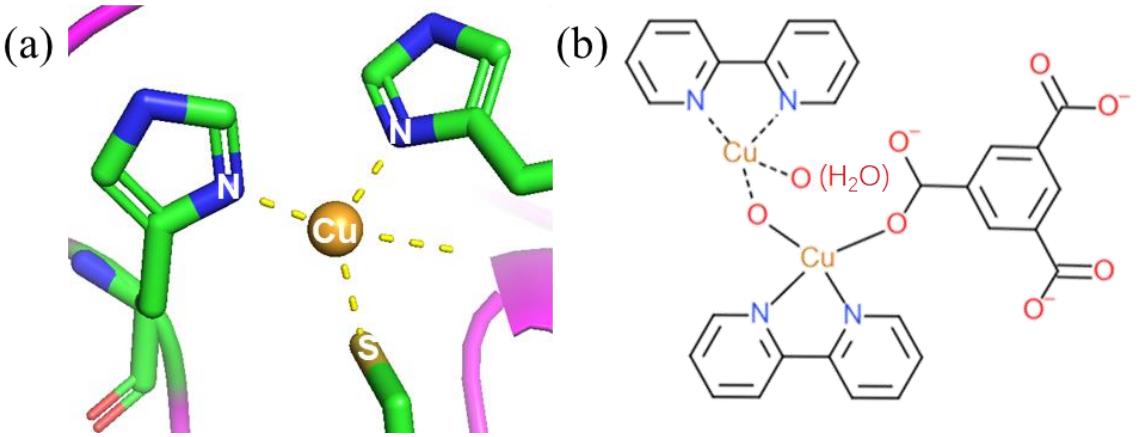

Figure 1. (a) T1copper and triangular coordinated atoms (two N atoms and one S atom) in laccase. (b) Structure of Cu-bipy-BTC MOF.

2. MATERIALS AND METHODS

2.1 Chemicals and Reagents

$(NH)_4S_2O_4$, sodium dodecyl sulfate (SDS) and trimeric acid were purchased from Beijing Solarbio Science & Technology Co. Ltd. (China). Bipyridine was purchased from Sigma-Aldrich (China). N_2 was purchased from Millennium Beijing Gas Co. Ltd. (Beijing, China). D-glucose was purchased from Sinopharm Chemical Reagent Co. Ltd. (Shanghai, China). The other chemical materials were purchased from Modern Orient (Beijing) Technology Development Co., Ltd. (China). All of the chemicals used were analytical reagent grade. All of the electrochemical materials were obtained from Tianjin Yida Heng Sheng Technology Development Co. Ltd. (China). Deionized water was used to prepare all aqueous solutions.

2.2 Characterization

Electrochemical analysis was performed on a CHI-853D electrochemical workstation (Shanghai Chenhua Instrument, China). A standard three-electrode system was used including a Au electrode (working electrode), Pt wire (counter electrode), and Ag/AgCl (reference electrode). Morphological investigations of the MOF were carried out by scanning electron microscopy (SEM) analysis (Merlin, Carl Zeiss, Jena, Germany). Energy dispersive spectrometry (EDS) characterization was also performed (Merlin, Carl Zeiss, Jena, Germany). Fourier-transform infrared (FTIR) spectra were recorded on a X70 instrument (NETZSCH, Germany). X-ray-diffraction (XRD) patterns were collected on an S2 instrument (Rigaku, Japan).

2.3 eElectrode Preparation

The surface of the Au electrode was first polished with 0.3-μm and then 50-nm alumina powder on chamois leather to obtain a mirror-like surface. Copper was then electroplated onto the surface of the electrode with a constant current. Next, $Cu(OH)_2$ was prepared on the surface using a previously published process [20]. Finally, the electrode was dipped into the reaction solvent for 4 min. The solvent was prepared by mixing 2,2-bipyridine (0.104 g), H_3BTC (trimesic acid) (0.092 g), NaOH (0.057 g), and acetic acid (0.08 mL) with 25 mL of water at 100°C. To our best knowledge, this is the first time Cu-bipy-BTC was prepared using a $Cu(OH)_2$ nanosheet. The preparation process is shown in Figure 2.

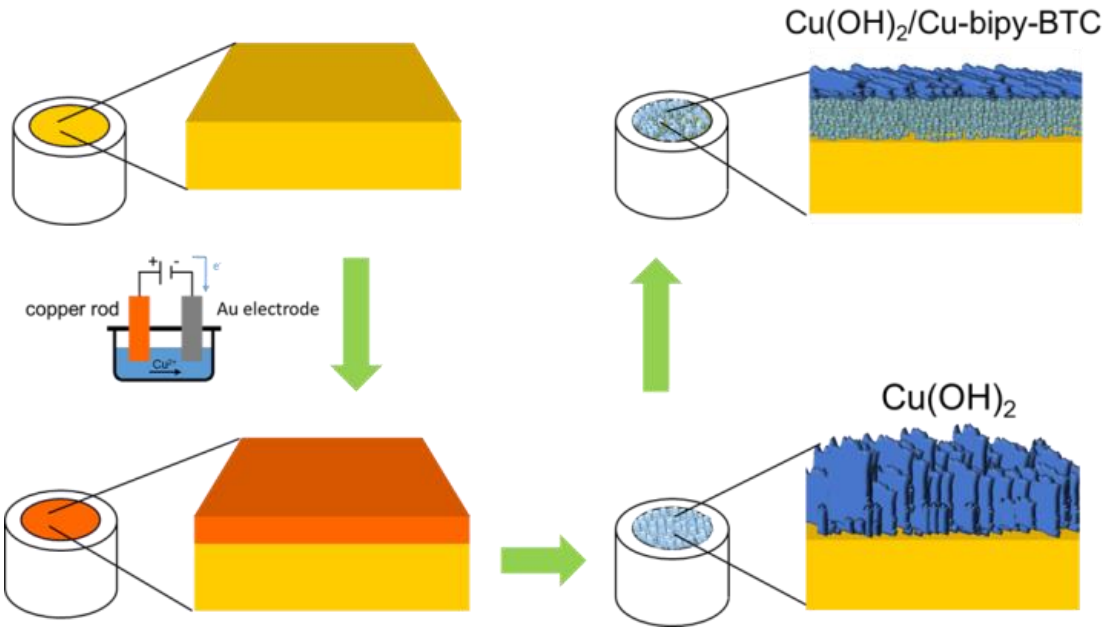

Figure 2. Preparation process of $Cu(OH)_2$/Cu-bipy-BTC on surface of Au electrode. First, Cu was electroplated onto the Au surface. Then, $Cu(OH)_2$ nanosheets were synthesized by reaction of Cu. Finally, $Cu(OH)_2$ nanosheets and Cu-bipy-BTC nanoparticles were obtained.

2.4 Analytical Procedure

Cyclic-voltammetry (CV) data were recorded between −0.75 and 0.75 V at a scan rate of 50 $mV \cdot s^{-1}$. All electrochemical experiments used a HAc/NaAc buffer solution (pH 5.5) as supporting electrolyte.

3. RESULTS AND DISCUSSION

3.1. Characterization on Surface of Electrode

Figure 3 shows the step-by-step preparation process: electroplating of Cu, synthesis of $Cu(OH)_2$, and preparation of Cu-bipy-BTC. The modified electrode surfaces at different steps were characterized by FT-IR, XRD, and EDS, with the results shown in the figure. In Figure 3(a), Cu-bipy-BTC exhibits a significant difference from $Cu(OH)_2$ and copper electroplating. A strong and wide band at approximately 3000–3500 cm^{-1} belongs to the υ(O-H) stretching vibration. The characteristic peak near 1610 cm^{-1} indicates the vibration of the benzene ring. The peak centered at 1560 cm^{-1} is attributed to υ(C-N). The stretching vibrations of υ_{as}(COO) and υ_{s}(COO) occurred at approximately 1360 cm^{-1}. The presence of the BTC and bipyridine is confirmed by all these findings. The above-mentioned results indicate that *in situ* fabricated Cu-bipy-BTC has a structure similar to that obtained by Jia *et al*. [18].

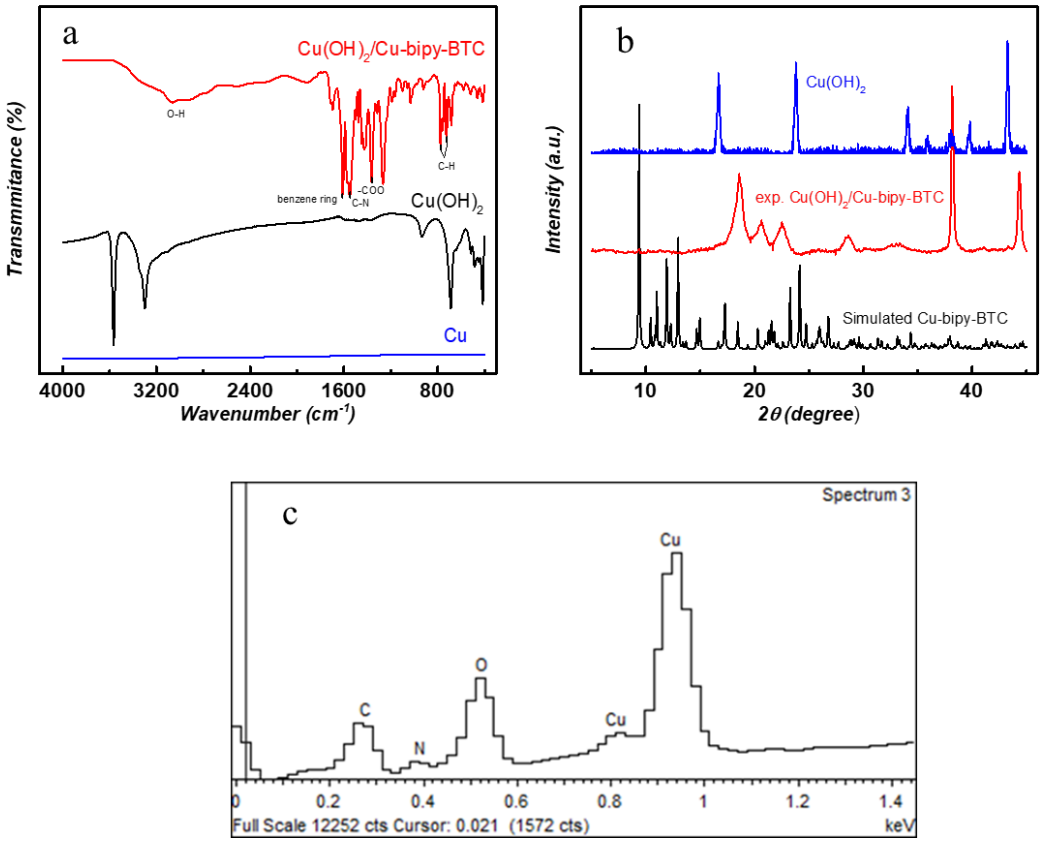

Figure 3. (a) FTIR curves of electrode surface during different steps in synthesis process: electroplating of copper, synthesis of $Cu(OH)_2$, and preparation of Cu-bipy-BTC. (b) XRD patterns of electrode surface: synthesis of Cu-bipy-BTC on electrode surface, simulation of Cu-bipy-BTC, and $Cu(OH)_2$. (c) EDS image of materials on electrode surface.

The chemical composition of the $Cu(OH)_2$/Cu-bipy-BTC on the electrode surface was determined by EDS [Figure 3(c)]. The peaks of C, O, N, and Cu indicate the synthesis of Cu-bipy-BTC. The practical molar ratio of Cu-bipy-BTC was Cu:C:N:O=1:2.8:0.7:2.1, and compared with the corresponding theoretical value of 1:14.5:2:4.5, shows less C, N, and O content due to the existence of $Cu(OH)_2$ in the electrode. Combining the results of Figures 3(a) and 1(c), it is indicated that Cu-bipy-BTC has been synthesized on the surface of the electrode.

Figure 3(b) shows the XRD pattern of the material on the electrode surface. There is no peak of Cu at 43.197°, which indicates that the Cu plated on the surface has been fully reacted in the second step to achieve $Cu(OH)_2$ nanosheets. At the same time, the results of Cu-bipy-BTC are different from $Cu(OH)_2$, which means that the further reaction to obtain Cu-bipy-BTC from $Cu(OH)_2$ has occurred. However, upon comparison with the case of simulated Cu-bipy-BT [18], the two XRD patterns were different, which was perhaps the result of different crystal structures and mixtures of $Cu(OH)_2$ and Cu-bipy-BTC. The mechanism of the structural difference could be caused by the micro-environment around the surface of the electrode during the synthesis process.

3.2. Structure on Surface of Electrode

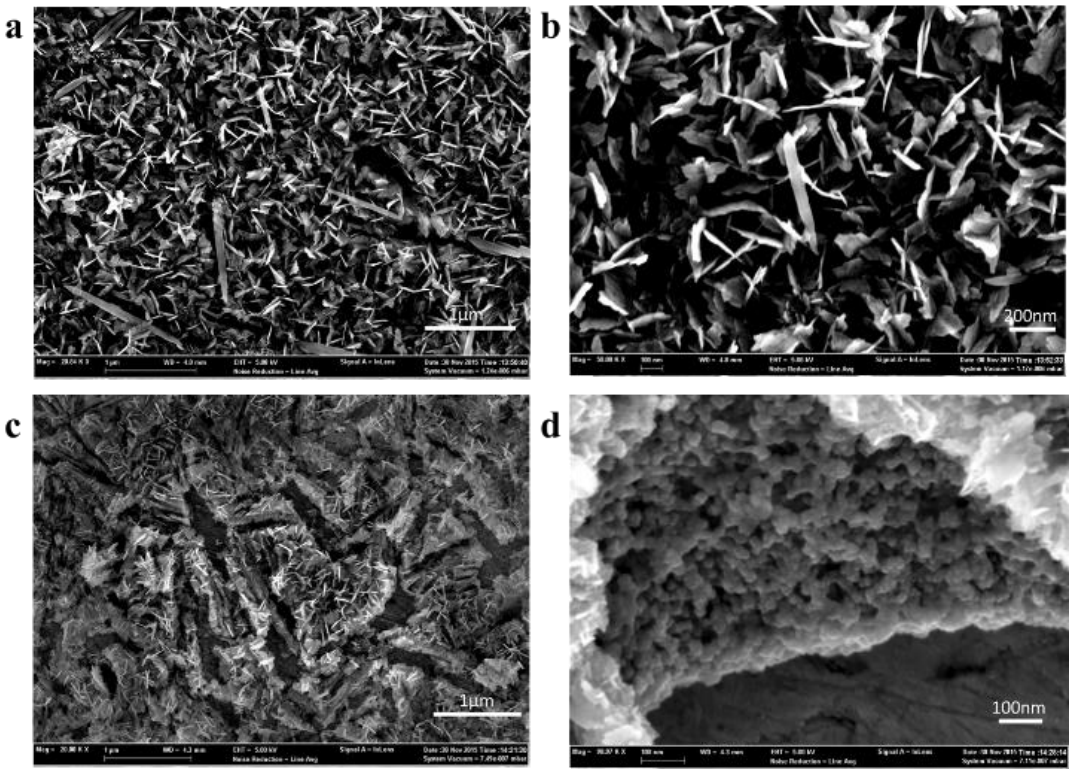

Figure 4. SEM image of materials on the electrode surface. (a) and (b) show the intermediate product, $Cu(OH)_2$, on the surface. (c) and (d) show the final structure on the surface.

SEM images of materials on the electrode surface are shown in Figure 4. Figures 4(a) and 4(b) show the $Cu(OH)_2$ structure during the preparation of the Cu-bipy-BTC electrode, and display a sheet-like structure and are consistent with the results from other works [20]. Figure 4(c) shows that the surface of the final product has a similar structure as the $Cu(OH)_2$ structure, but there are numerous cracks distributed on the surface. The length of the crack is approximately 1 μm and the width 100–200 nm. At the bottom of cracks, one can see the Au plate as shown in Figure 4(d). A magnified image [Figure 4(d)] shows that some small particles approximately 10 nm in size exist at the structure of inner cracks. The sizes of such particles are smaller than the size obtained by the hydration method. From the EDS results and synthesis process, it can be deduced that the structure may be the combination of $Cu(OH)_2$ and Cu-bipy-BTC crystals. On one hand, the synthesis $Cu(OH)_2$ was the reactant of Cu-bipy-BTC. On the other hand, the Cu-bipy-BTC grows on the cracks formed by $Cu(OH)_2$. It is concluded that the special MOF structure formed on the electrode, namely, the surface is a lamellar structure composed of $Cu(OH)_2$ and the inner is composed of small Cu-bipy-BTC paritcles. Such structure could also explain the different results in Figures 3(a) and 3(b).

3.3. Basic Electrochemical Investigation

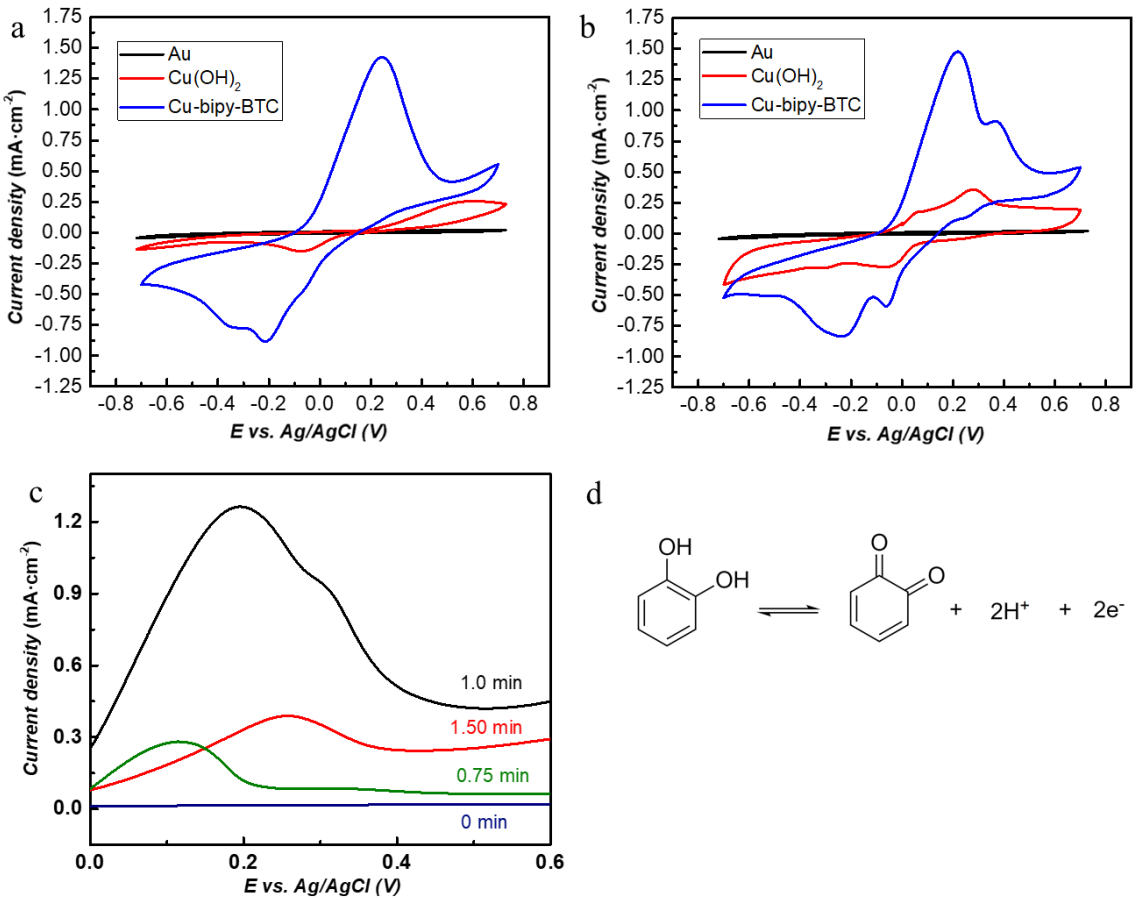

Figure 5. (a) CV curves for Au, $Cu(OH)_2$, and Cu-bipy-BTC in 20-mM HAc/NaAc buffer solution (pH 5.5) at scan rate of 50 $mV \cdot s^{-1}$. (b) CV curves for Au, $Cu(OH)_2$, and Cu-bipy-BTC in 20-mM HAc/NaAc buffer solution (pH 5.5) containing 1-mM catechol at a scan rate of 50 $mV \cdot s^{-1}$. (c) CV curves of Cu-bipy-BTC electrode with different electroplating times in 20-mM HAc/NaAc buffer solution (pH 5.5). (d) Probable mechanism of oxidation of catechol.

The electrochemical properties of the electrode were studied in 20-mM Hac/NaAc buffer solution by CV measurements. Figure 5(a) shows that $Cu(OH)_2$/Cu-bipy-BTC has an anodic peak at 0.3 V corresponding to the oxidation of Cu(II), and an acathodic peak at approximately –0.3 V corresponding to the reduction of Cu(II). Compared with the $Cu(OH)_2$ electrode, the current for the Cu-bipy-BTC electrode is much higher and the peaks are in low-voltage positions, indicating better electrochemical activity and different electrochemical behavior. Compared with the Cu atom positions in $Cu(OH)_2$/Cu-bipy-BTC and laccase as shown in Figure 1, one can assume that the enzyme-like environment around Cu with the MOF is the main reason for such differences. This $Cu(OH)_2$/Cu-bipy-BTC electrode can be used in the catalysis and detection of catechol, which is the substrate of laccase. The electrochemical activities of Au, $Cu(OH)_2$, and Cu-bipy-BTC for catechol were studied by CV in 20-mM HAc/NaAc buffer solution (pH 5.5) with 1-mM catechol at scan rate of 50 $mV \cdot s^{-1}$ as shown in Figure 5(b). The CV response has a new oxidation peak at +0.4 V (versus Ag/AgCl), corresponding to the oxidation of catechol. The probable reaction mechanism is shown in Figure 5(d), and catechol reacted into

benzoquinone. As for $Cu(OH)_2$, although there was a similar reponse to catechol, the peak was much smaller than that of Cu-bipy-BTC. Thus, the activity of catechol on the surface of the electrode is dependent on the special structure of Cu-bipy-BTC, and the different environments of Cu enhanced the electrochemical oxidation activity of catechol.

In addition, the electrochemical behavior of electrodes fabricated with different electroplating times was further investigated in 20-mM/L HAc/NaAc buffer solution (pH 5.5), as shown in Figure 5(c). It can be seen from the results that the best electroplating time is 1 min as that results in the largest peak current, and an overly long or overly short time might cause the decrease of peak current. The electroplating time will influence the thickness of Cu on the surface, and further affect the synthesis of Cu-bipy-BTC. When the electroplating time is too long, the Cu-bipy-BTC on the surface is too thick, leading to an increase of resistance. When the time is too short, there is little Cu-bipy-BTC on the surface, leading to the decrease in thickness of the catalytic center.

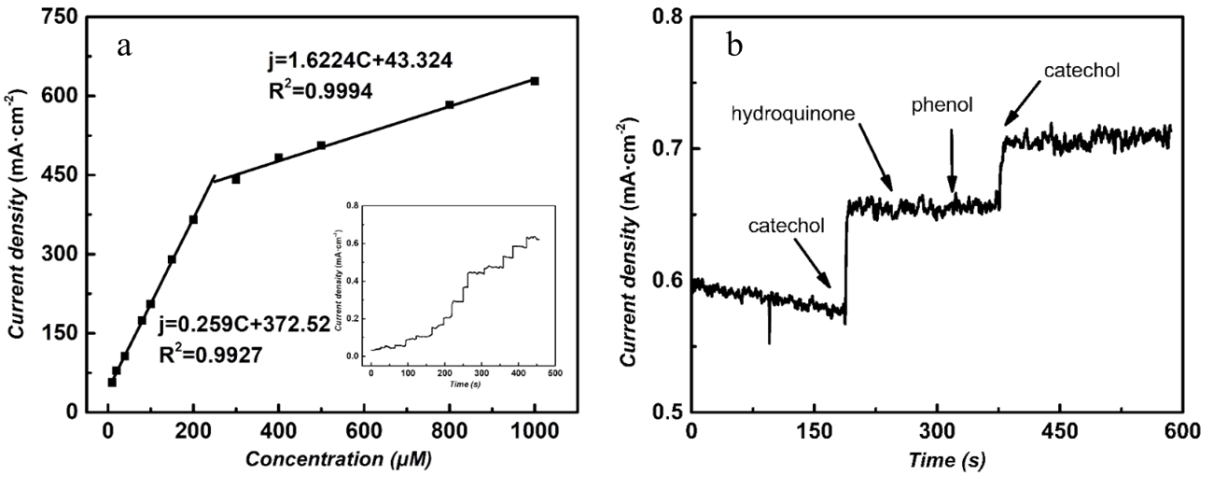

Figure 6. (a) Relationship between current response and catechol concentration at +0.4 V (vs. Ag/AgCl) in 20-mM HAc/NaAc buffer solution (pH 5.5). (b) Selectivity for catechol (1 mM) in the presence of methylbenzene (1 mM) and phenol (1 mM).

The quantitative detection of catechol with Cu-bipy-BTC was investigated by plotting *i-t* curves for various concentrations of catechol at +0.4 V. Figure 6(a) shows the relationship between current response and catechol concentration. The stripping currents increase linearly with catechol concentration covering two ranges, i.e., 10–250 μM (R^2=0.994) and 250–1000 μM^{-1} (R^2=0.9927), with a detection limit of 4.69 μM (S/N=3). The sensitivities are 1.6224 $\mu A \cdot cm^{-2} \cdot \mu M^{-1}$ in the range 10–250 μM and 0.2591 $\mu A \cdot cm^{-2} \cdot \mu M^{-1}$ in the range 250–1000 μM. The two sectional linear regions shown in Figure 6(a) could be explained as follows. At low concentration (< 250 μM), the number of unoccupied activation sites of Cu-bipy-BTC are sufficient. Catechol reacts to create product rapidly and the surface of the electrode is depleted quickly, leading to high sensitivity. However, the surface fouled by products limits the detection of catechol, so it is less sensitive to increasing concentration. Similar results were also found in other studies [21,22].

For a catechol sensor, the noise from other phenolic compounds is important for the detection of catechol. Methylbenzene and phenol are common phenolic compounds in polluted water [23]. A total of 1 mM methylbenzene and 1 mM phenol were added to check the selectivity. Figure 6(b) shows that the electrode has no response to methylbenzene and phenol. Even in the presence of methylbenzene and phenol, this MOF electrode still has high sensitivity to catechol.

Table 1. Detection of catechol in tap water samples.

Sample		Detected (μM)	Added (μM)	Found (μM)	Recovery (%)
Tap water	1	0	50	52.8	105.6
	2	0	300	297.3	99.1
	3	0	500	505.6	101.1

To evaluate the applicability of Cu-bipy-BTC for catechol, tap water was used as real sample. No catechol was found in the origin sample by our electrode. Then 50-μM, 300-μM and 500-μM catechol were added and different samples were analyzed by our catechol. Recovery of each sample was calculated based on detected results. As shown in Table 1, recovery of catechol was range from 99.1% to 105.6% which indicates reliable detection of catechol by Cu-bipy-BTC electrode.

Table 2. Comparison of linear range, sensitivity, and LOD (limit of detection) of enzymatic or non-enzymatic catechol sensors.

Modified electrode	Linear range (μM)	Sensitivity ($\mu A \cdot cm^{-2} \cdot \mu M^{-1}$)	LOD (μM)	Ref.
Nafion/laccase/ACZUF	0.166–7	0.023	0.17	[24]
Laccase/PVA-AWP/SPE	0.5–175	0.1569	0.56	[25]
Laccase/*E. coli* cells/GC	0.5–300	-	0.1	[26]
Cu-OMC/CS/Laccase/Au	0.67–15.75	0.104	0.67	[27]
Lac/AP-rGOs/Chit/GCE	15–700	0.0158	7.00	[28]
$Cu_3(btc)_2$/CS-ERGO/GCE	2–200	0.7869	0.41	[29]
MOF-ERGO-5/GCE	0.1–556	0.5343	0.10	[30]
GQD/GCE	6.0–400	0.9766	0.75	[31]
TiO_2/C_{900}/GCE	5–300	0.136	2.05	[32]
ZIF-8C/rGO/GCE	0.5–10	1.17	0.073	[22]
	10–70	0.47		
Cu-bipy-BTC/Au	10–250	1.6224	4.69	This work
	250–1000	0.2591		

Comparison results for the Cu-MOF electrode prepared *in situ* with other enzymatic electrodes that used laccase or other non-enzymatic electrodes with the MOFs mainly employed are listed in Table 2. From the table, it can be found that non-enzymatic sensors are better than enzymatic sensors. Upon comparison with the non-enzymatic sensor, the electrode in this work presents a wider linear range, higher sensitivity, and the LOD can meet the detection requirements.

4. CONCLUSIONS

In conclusion, a novel hybrid non-enzymatic electrode composed of Cu(OH)2 nanosheets and Cu-bipy-BTC MOF nanoparticles was fabricated to detect catechol. This hybrid structure can be in situ grown directly on the surface of a Au electrode that was electroplated with Cu under specific conditions. Cu-bipy-BTC MOF nanoparticles, which are embedded in the hydrophobic environment formed by Cu(OH)2 nanosheets, function as active sites for catalyzing the oxidation of catechol. This hybrid structure mimics the active site of laccase, exhibiting high activity and sensitivity. The MOF electrode enables the catalytic oxidation of catechol at +0.4 V (versus Ag/AgCl). The amperometric responses are linear with concentrations of catechol ranging from 10 to 250 μM and from 250 to 1000 μM with sensitivities of 1.6224 and 0.2591 μA·cm–2·μM–1, respectively. The electrode also shows selectivity for methylbenzene and phenol. Compared with other catechol electrochemical sensors, the MOF-based electrode developed has advantages of higher sensitivity and ease of fabrication. The reliable detection results in practical samples show potential application in the detection of catechol.

AUTHOR CONTRIBUTIONS

Conceptualization, D.L and L.R; methodology, Z.L. and L.R; validation, Z.L., L.R. and D.L.; formal analysis, Z.L.; investigation, Z.L.; resources, Z.L.; data curation, Z.L. and L.R.; writing—original draft preparation, Z.L.; writing—review and editing, D.L.; visualization, Z.L.; supervision, D.L.; project administration, D.L.; funding acquisition, D.L."

FUNDING

This work is supported by the National Natural Science Foundation of China under grant No. U1862204 and No. 21878175, and by the National Key Research and Development Program of China under Grant No. 2018YFA0902200

ACKNOWLEDGMENTS

This work is supported by the National Natural Science Foundation of China under grant No. U1862204 and No. 21878175, and by the National Key Research and Development Program of China under Grant No. 2018YFA0902200.

CONFLICTS OF INTEREST

The authors declare no conflict of interest.

References

1. F. Xu, *Biochemistry*, 35 (1996) 7608.
2. N. Duran and E. Esposito, *Applied Catalysis B: Environmental*, 28 (2000) 83.
3. H. Claus, *Micron*, 35 (2004) 93.
4. K. Piontek, M. Antorini, and T. Choinowski, *J Biol Chem*, 277 (2002) 37663.
5. H. B. Gray, B. G. Malmström, and R. J. Williams, *J Biol Inorg Chem*, 5 (2000) 551.
6. N. Schweigert, A. J. Zehnder, and R. I. Eggen, *Environ Microbiol*, 3 (2001) 81.
7. M. Rodríguez, G. Aleman, J. Rodriguez-Delgado, G. Dieck-Assad, S. O. Martinez-Chapa, D. Barceló, and R. Parra, *TrAC Trends in Analytical Chemistry*, 74 (2015) 21.
8. K. Wang, J. Tang, Z. Zhang, Y. Gao, and G. Chen, *Electrochimica Acta*, 70 (2012) 112.
9. H. Zhang and A. G. Hay, *Journal of Hazardous Materials*, 384 (2020) 121272.

10. O. M. Yaghi and H. Li, *Journal of the American Chemical Society*, 117 (1995) 10401.
11. M. Safaei, M. M. Foroughi, N. Ebrahimpoor, S. Jahani, A. Omidi, and M. Khatami, *TrAC Trends in Analytical Chemistry*, 118 (2019) 401.
12. M. Zhao, S. Ou, and C.-D. Wu, *Accounts of Chemical Research*, 47 (2014) 1199.
13. L.-F. Song, C.-H. Jiang, C.-L. Jiao, J. Zhang, L.-X. Sun, F. Xu, W.-S. You, Z.-G. Wang, and J.-J. Zhao, *Crystal Growth & Design*, 10 (2010) 5020.
14. J. Mao, L. Yang, P. Yu, X. Wei, and L. Mao, *Electrochemistry Communications*, 19 (2012) 29.
15. G. Jia, W. Zhang, Z. Jin, W. An, Y. Gao, X. Zhang, and J. Liu, *Electrochimica Acta*, 144 (2014) 1.
16. L. Zhang, Y. Hu, J. Chen, W. Huang, J. Cheng, and Y. Chen, *Journal of Power Sources*, 384 (2018) 98.
17. C. Jun-feng, C. Yuan-cai, C. Jian-hua, H. Yong-you, H. Wan-tang, and Z. Li-hua, *Journal of Electrochemistry*, 25 (2019) 511.
18. G. Jia, Y. Gao, W. Zhang, H. Wang, Z. Cao, C. Li, and J. Liu, *Electrochemistry Communications*, 34 (2013) 211.
19. A. Ehsani, J. Khodayari, M. Hadi, H. M. Shiri, and H. Mostaanzadeh, *Ionics*, 23 (2017) 131.
20. W. Zhang, X. Wen, S. Yang, Y. Berta, and Z. L. Wang, *Advanced materials*, 15 (2003) 822.
21. A. Gholizadeh, S. Shahrokhian, A. Iraji zad, S. Mohajerzadeh, M. Vosoughi, S. Darbari, J. Koohsorkhi, and M. Mehran, *Analytical Chemistry*, 84 (2012) 5932.
22. H. Chen, X. Wu, C. Lao, Y. Li, Q. Yuan, and W. Gan, *Journal of Electroanalytical Chemistry*, 835 (2019) 254.
23. W. W. Anku, M. Mamo, and P. Govender, *Phenolic Compounds in Water: Sources, Reactivity, Toxicity and Treatment Methods*. 2017. p. 420-443.
24. X. Chen, D. Li, G. Li, L. Luo, N. Ullah, Q. Wei, and F. Huang**, *Applied Surface Science*, 328 (2014) 444.
25. P. Ibarra-Escutia, J. J. Gómez, C. Calas-Blanchard, J. L. Marty, and M. T. Ramírez-Silva, *Talanta*, 81 (2010) 1636.
26. Z. Zhang, J. Liu, J. Fan, Z. Wang, and L. Li, *Analytica Chimica Acta*, 1009 (2018) 65.
27. X. Xu, M. Guo, P. Lu, and R. Wang, *Materials Science and Engineering: C*, 30 (2010) 722.
28. X. Zhou, L. Liu, X. Bai, and H. Shi, *Sensors and Actuators B: Chemical*, 181 (2013) 661.
29. Y. Yang, Q. Wang, W. Qiu, H. Guo, and F. Gao, *The Journal of Physical Chemistry C*, 120 (2016) 9794.
30. Q. Chen, X. Li, X. Min, D. Cheng, J. Zhou, Y. Li, Z. Xie, P. Liu, W. Cai, and C. Zhang, *Journal of Electroanalytical Chemistry*, 789 (2017) 114.
31. X. Yuan, D. Yuan, F. Zeng, W. Zou, F. Tzorbatzoglou, P. Tsiakaras, and Y. Wang, *Applied Catalysis B: Environmental*, 129 (2013) 367.
32. Z. Wang, M. Li, Y. Ye, Y. Yang, Y. Lu, X. Ma, Z. Zhang, and S. Xiang, *Journal of Solid State Electrochemistry*, 23 (2019) 81.